Engineering Journal issn: 0125-8281

Article

Verifying the Reliability of Impressed Current Method to Simulate Natural Corrosion in Reinforced Concrete

Thi Hai Yen Nguyen[1,*], Van Hong Linh Bui[1], Van Mien Tran[2,3], Nguyen Thi Cao[4], Withit Pansuk[5], and Pitcha Jongvivatsakul[5]

1 Department of Civil Engineering, Industrial University of Ho Chi Minh City, 12 Nguyen Van Bao, Ward 4, Go Vap Dist, Ho Chi Minh 700000, Vietnam
2 Faculty of Civil Engineering, Ho Chi Minh City University of Technology (HCMUT), 268 Ly Thuong Kiet Street, District 10, Ho Chi Minh City, 70000, Vietnam
3 Vietnam National University Ho Chi Minh City, Linh Trung Ward, Thu Duc District, Ho Chi Minh City, 70000, Vietnam
4 Faculty of Civil Engineering, Tien Giang University, 119 Ap Bac, ward 5, My Tho city, Tien Giang 860000, Vietnam
5 Innovative Construction Materials Research Unit, Department of Civil Engineering, Faculty of Engineering, Chulalongkorn University, 254 Phayathai Road, Pathumwan, Bangkok 10330, Thailand
*E-mail: nguyenthihaiyen@iuh.edu.vn (corresponding author)

Abstract. In order to accelerate the corrosion of steel reinforcement in the reinforced concrete structures for laboratory research, the impressed current method has been used widely regardless of the appropriacy of this method on the various aims of the studies relating to the deterioration of the reinforced concrete structures. The aim of this study is to characterize the influence of the impressed current method on the steel-concrete interface in the reinforced concrete to verify the reliability of this method on simulating the natural corrosion. The mill-scale of the steel reinforcement and the steel-concrete interfacial region were investigated using SEM-EDS. The results indicate that impressed current can induce the non-uniform and localized corrosion on the steel reinforcement. The corrosion products formed were likely to the natural corrosion induced by chloride environments. However, the oxidization of OH^- at anode can inhibit the precipitation of corrosion products at steel-concrete interfacial region and then slowing down the formation of crack in concrete. This positively leads to an overestimation of load capacity of corroded structure and raises doubt on utilizing this technique to simulate the corrosion behavior.

Keywords: Impressed current method, corrosion products, mill-scale, corrosion.

ENGINEERING JOURNAL Volume 25 Issue 3
Received 21 December 2020
Accepted 12 March 2021
Published 31 March 2021
Online at https://engj.org/
DOI:10.4186/ej.2021.25.3.105

DOI:10.4186/ej.2021.25.3.105

1. Introduction

Reinforced concrete is the most used material in construction where the steel reinforcement is supposed to be protected well in alkaline environment generated by concrete. Unfortunately, concrete is heterogeneous material with various pore sizes that can permit aggressive agents from exposure penetrating into concrete, reaching the steel surface and then triggering the corrosion of steel reinforcement [1-2]. The corrosion of steel in reinforced concrete structure is one of the most critical issues leading to the deterioration of reinforced concrete structure and consequently shortening the service lifetime of the structure [3], particularly those expose chloride environments [4-6]. Generally, the corrosion process of steel in reinforced concrete structure can last for several years or decades [1, 4, 6]. From the engineering viewpoint, the service life of a reinforced concrete structure includes two stages, initiation stage and propagation stage. The initiation stage begins with the adequate accumulation of aggressive agents such as chloride ions or the reduction of pH of concrete's pore solution at steel-concrete interface [1, 4, 6], triggering the corrosion of steel by depassivating the stable mill-scale on steel surface. The depassivation of the mill-scale is considered to be a mark for the beginning of the propagation stage where the corrosion of steel is initiated and then forms various types of corrosion products. Each type of corrosion products owns different specific volume that are about 2 to 6.5 times higher compared to the original volume of steel lost [7]. Depending upon the exposure condition, the types of corrosion products and their ratios are varied, leading to the different change of volume increasing. The accumulation of adequate corrosion products at steel-concrete interface can generate expansive pressure and induce the cracks in concrete, which can expand to the concrete surface, and then speeding the ingress of aggressive agents into concrete, leading to serious damage of reinforced concrete structure. Due to the importance and the worldwide extent of steel-corroded issue in reinforced concrete structure, it has drawn much attention. Numerous research including both experiments as well as simulation have been carried out in order to comprehend the corrosion mechanism, factors affecting corrosion process [7-10] as well as binder characteristic that affect the penetration of aggressive agents [11-15]. They are greatly important for the prediction of the durability and service lifetime of reinforced concrete structure. Based on that, the maintenance of deteriorated structure can be taken on time and the service life of the structure can be prolonged with various rehabilitation methods [16-18].

While the corrosion process of steel reinforcement lasts for several years, the time frame of a research project is usually limited, causing the main obstruction for research those taken on natural corrosion. Therefore, it is a demand to develop the methods that can accelerate the corrosion process of the steel reinforcement in the reinforced concrete structure. There are several methods have been invented to serve for that purpose but essentially can be categorized as two corrosion-accelerated techniques. One utilizes the artificial climate environment and other uses the impressed current method. The impressed current method has been developed based on Faraday's second law, as shown in Eq. (1), where steel reinforcement is connected to positive electrode (anode) and cathode is connected to a counter electrode.

$$\Delta m = \frac{MIt}{zF} \quad (1)$$

where: Δm : mass of steel consumed (g)
M : atomic weight of steel (56 for Fe)
I : average electric current (A)
t : time (s)
F : Faraday's constant = 96480 (A/s)
z : ionic charge (= 2)

The proportional correlation between the mass loss of corrosion and the time of electrical current application is probably the most outstanding advantage of this method, making it to be the useful method for research needing the acceleration of the corrosion process in order to investigate the deterioration of reinforced concrete structure with respect to the generation of crack in concrete [19-21], the mass loss due to corrosion [22-23] as well as predicting the lifetime of reinforced concrete structure [24-27]. Although numerous research have used the impressed current method to accelerate the corrosion of reinforced concrete structure for various study purposes, it is still unclear if the impressed current method can be fully able to simulate the interaction between corrosion products of steel rebar and cement paste at the steel-concrete interface [24, 28-30]. It is considered that the impressed current method is unable to generate non-uniform corrosion, which usually happens in reinforced concrete structure at first stage of corrosion process, particularly the structure exposed chloride environment. Some researchers have concluded this method cannot be able to representative the mechanical behavior of structure and the uniform corrosion can lead to the overestimation of structure's load capacity [24, 30]. Moreover, the mill-scale exists on the steel surface before the steel reinforcement is embedded in concrete. Although its chemical compositions are iron oxide, it should not be considered as the type of rust. Instead, the thickness, intact condition as well as the distribution of mill-scale should be tactfully examined to evaluate the capacity of it on protecting the steel substrate beneath.

Due to this controversial reason, the primary aim of this research is to characterize the deterioration of mill-scale of steel reinforcement and the penetration of corrosion products into concrete in order to verify the reliability of the impressed current method on simulating the deterioration of reinforced concrete structure caused by the natural corrosion. To do that, the microstructure and chemical composition of the steel surface before and

after conducting the impressed current were taken and compared to examine the change of the mill-scale on steel surface. Furthermore, the interaction between corrosion products formed and concrete at the steel-concrete interface was tactfully investigated.

2. Experimental Program

Reinforced concrete prisms with the size of 100x100x150 mm were cast. A steel bar with diameter and length of 20x130 mm was placed at the center of the prism. The reinforcement used was hot-rolled deformed steel SD390 in accordance to JIS G3112:2020. Schematic of reinforced concrete prism is shown in Fig. 1. Concrete with the water-to-cement ratio of 0.5 and compressive strength of 30 MPa was prepared with maximum coarse aggregate of 20 mm. Cement with chemical composition and properties as shown in Table 1 and Table 2 were used. The proportion of concrete mixture is presented in Table 3. The reinforced concrete prisms were casted and demolded one day after casting. These prisms were cured for 13 days in water.

The prisms were then set up for the corrosion acceleration. They were immersed in 3.5% sodium chloride solution for 2 days to ensure the full saturation. The impressed current of 300 μA/cm² was applied within 360 hours in order to generate the mild corrosion of the steel bar. With that application, the impressed current theoretically generated a corrosion degree of 3% wt., which is equivalent to approximately 140-μm section loss of steel bar. At this corrosion degree, it is supposed to be the beginning of the propagation stage of design service life of reinforced concrete structure where the crack can be formed at the steel-concrete interface though the bond strength may insignificantly reduce [31]. The laboratory setup for accelerating the corrosion is shown in Fig. 2.

After the corrosion acceleration was done, the reinforced concrete prisms were sliced by a cutter with diamond saw at very low speed along the horizontal direction of the steel rebar to examine the visible formation of rust. The samples were then cut onto the size of 40x40x3 mm, as shown in Fig. 3. They were dried in desiccator for 3 days before impregnated with low viscosity resin. The impregnated sample were ground with SiC abrasive paper with the grades of 280, 400, 800 and 1200. Then they were polished with diamond suspensions with the sizes of 9 μm, 6 μm and 3μm. 2-iso propanol were used as lubricant for whole process of grinding and polishing. After polishing, the impregnated samples were cleaned by ultrasonic cleaner for 10 minutes with 2-isopropanol. They were dried in desiccator for 3 days and then restored in the vacuum chamber. The samples were coated with carbon before carrying out scanning electron microscopy analysis (SEM).

In this study, SEM analysis was implemented with backscattered electron (BSE) mode coupled with energy Dispersive X-Ray Spectroscopy (EDS) on FEI Quanta 50 SEM. The EDS experiment was operated with the accelerating voltage of 15 kV. The ratios of elements were obtained in terms of atomic ratios.

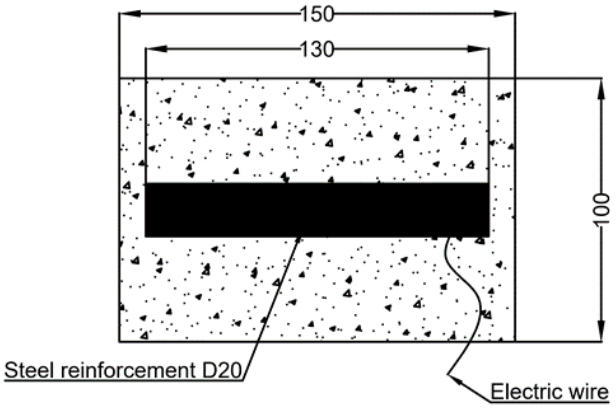

Fig. 1. Schematic of the reinforced concrete prism (dimension in mm).

Table 1. Chemical compositions of cement (% wt).

SiO_2	21.9
Al_2O_3	5.2
CaO	64.4
Fe_2O_3	3.1
MgO	1.4
SO_3	1.7
Na_2O	0.2
K_2O	0.4
TiO_2	0.2
MnO	0.3
I.L	2.26

Table 2. Physical properties of cement.

Specific gravity	Blaine fineness (cm^2/g)	Strength (MPa)		
		3 days	7 days	28 days
3.16	3340	30.3	45.1	61.6

Table 3. Proportion of concrete.

Water/cement ratio	Cement (kg/m^3)	Fine aggregate (kg/m^3)	Coarse aggregate (kg/m^3)
0.5	430	735	1183

DOI:10.4186/ej.2021.25.3.105

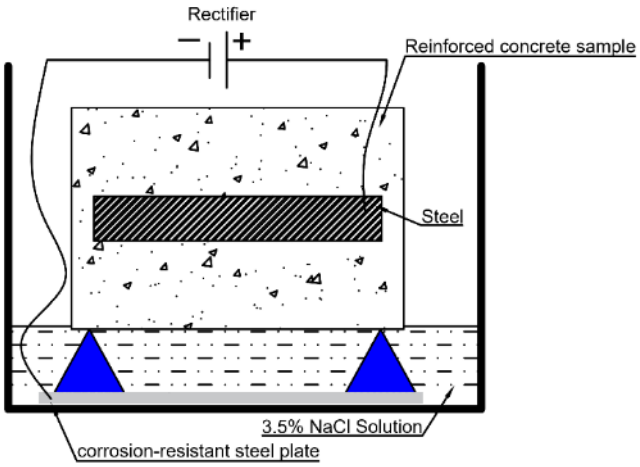

Fig. 2. Laboratory setup for impressed current application.

Fig. 3. Sample prepared for SEM-EDS observation on non-corroded steel specimen.

3. Results and Discussions

3.1. Mill-Scale Before Applying Impressed Current

Figure 4 shows the SEM image of the mill-scale on the surface of steel rebar at various positions before applying the impressed current to accelerate the corrosion process. It can be seen that the mill-scale distributes uniformly on the surface of the steel reinforcement with the thickness of 15-20 μm.

The high magnification of SEM images, as shown in Fig. 5, exhibit that the mill-scale on the surface of steel substrate is not fully intact but appears randomly fractured. These fractured defects are likely to be an initially imperfect characteristic of mill-scale of steel reinforcement [10] though the cutting process for the sample preparation or the transportation and preservation of steel may cause some minor defects such as the occurrence of rust spots or scratches on the steel surface before using in reinforced concrete.

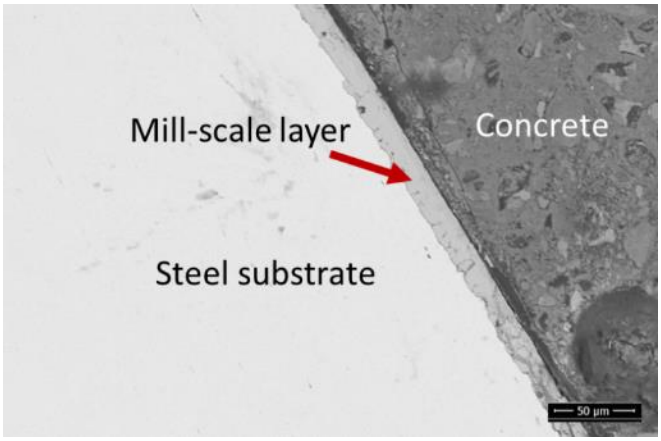

Fig. 4. Distribution of mill-scale on steel reinforcement surface of non-corroded sample.

Furthermore, Fig. 5 also expresses that the mill-scale includes two layers distinguished by the brightness level. They are assigned as layer I and layer II, as indicated clearly in Fig. 5(a). The layer I is directly next to the steel substrate and brighter than the layer II, which located at the outermost on the surface of the steel reinforcement. The thickness of the layer I is approximately 11-15 μm. EDS spot analyses indicated that the layer (I) was made of iron oxides with the Fe/O ratios of 1.02±0.08. This oxide layer is possibly Wustite (FeO) which was formed on the surface of the steel rebar during some first seconds it exposed the atmosphere during the hot rolling manufacture [32].

Similarly, the layer II with the thickness of approximately 5 μm was also made of iron oxide. However, the Fe/O ratios in layer II was more diverse than that in the layer I and depending on the spot locations the EDS took place. Based on the spot location, the layer II can be distinguished into two sublayers, addressed as sublayer II-1 and sublayer II-2. Although the boundary of these sublayers is hardly to specify clearly, the sublayer II-1 located beside the layer I with the Fe/O ratio of 0.815±0.035. Nevertheless, the sublayer II-2 was on the outermost of the steel surface and possessed lower Fe/O ratio compared to the sublayer II-1, approximately 0.715±0.025. The thicknesses of sublayer II-1 and sublayer (II-2) were about 2.5-3.2 and 0.75-1.05 μm, respectively. Based on the preliminary studies [30, 32], the sublayer II-1 is probably a mixture of Wustite FeO and Magnetite Fe_3O_4 while the sublayer II-2 is possibly magnetite Fe_3O_4 or a mixture of magnetite Fe_3O_4 and hematite α-Fe_2O_3. Obviously, the superior oxidization states of iron in the layer II located on the surface of steel reinforcement are subsequence of the grain grown originally from Wustite due to hot rolling manufacture exposing the atmosphere [32, 33].

Considering the steel-concrete interfacial region, the greater porosity distributed along the steel-concrete interface is observed, as shown in Fig 4 and Fig. 5. That is a typical feature of the steel-concrete interface and strongly affects the free-expansion period at the initiation stage of corrosion process in the reinforced concrete structure, where corrosion products can accumulate without causing cracks in concrete at the interface before reaching the propagation stage. Besides, the process of sample preparation may wash Portlandite, a highly soluble phase in concrete, accumulated at that transition zone, leading to higher porosity at this region.

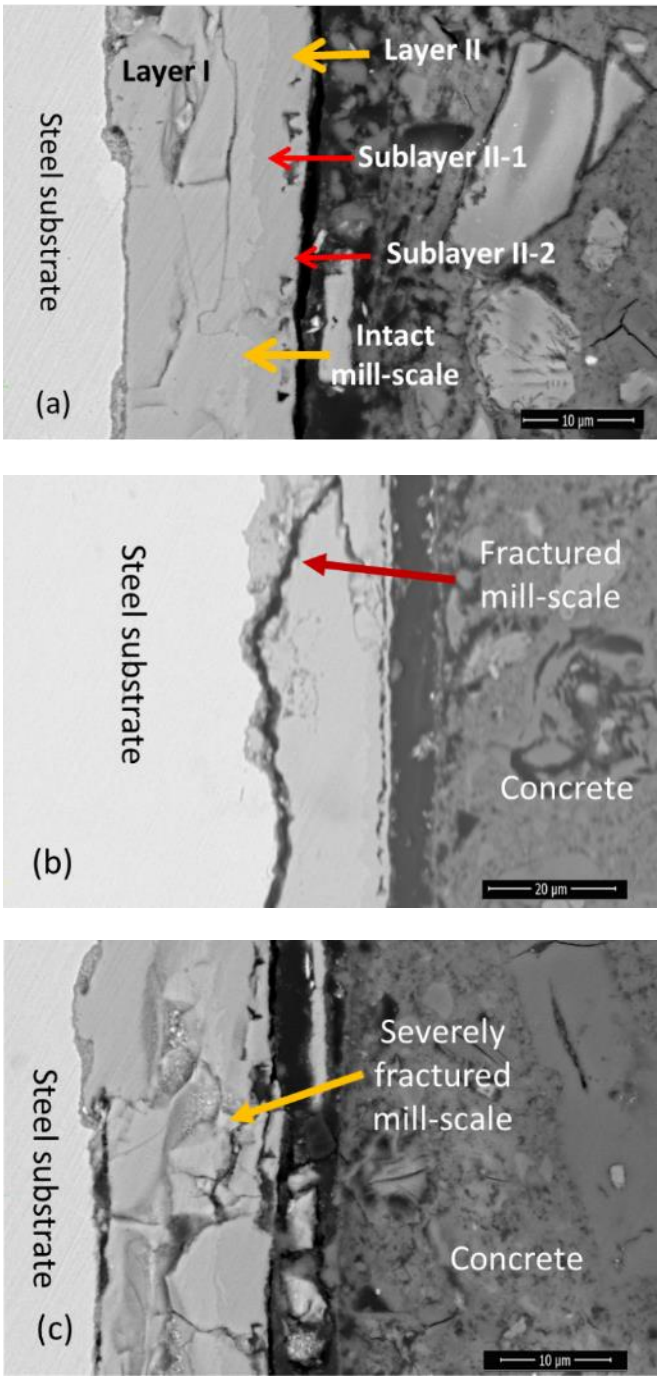

Fig. 5. Mill-scale on steel surface of non-corroded sample (a) intact mill-scale, (b) fractured mill-scale, and (c) severely fractured mill-scale.

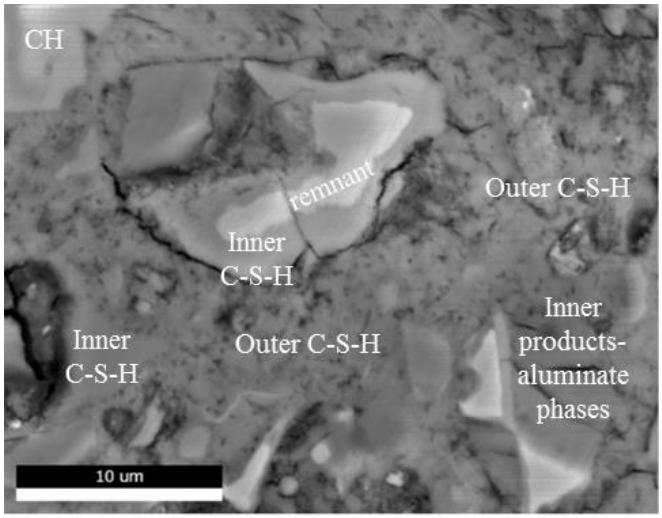

Fig. 6. Cement paste at steel-concrete interfacial region before applying impressed current.

The cement paste at the region near the steel-concrete interfacial region contains remnants of cement particles, calcium silicate hydrate phase (C-S-H), Portlandite, and aluminate hydrate phases, as presented in Fig. 6. C-S-H existed plentifully with the C/S ratios of 1.6-2.2, approximately. There was insignificant difference of C/S ratio in C-S-H phase between outer and inner products.

3.2. Mill-scale and Rust Distribution After Applying Impressed Current

Fig. 7 presents the steel-concrete interfacial region after the impressed current was employed to induce the corrosion on the steel reinforcement. Visual examination indicates that the corrosion induced by the impressed current method is non-uniform. It happened to be more severe on one side of steel reinforcement which directly faced the NaCl solution (cathode) during the application of electric current, called side (2), compared to the other side, assigned as side (1).

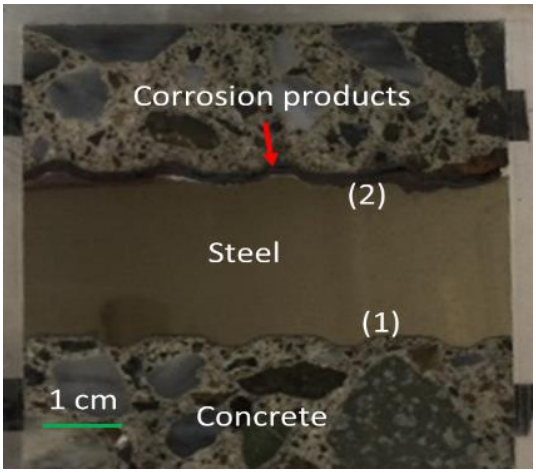

Fig. 7. Steel-concrete region after applying impressed current.

DOI:10.4186/ej.2021.25.3.105

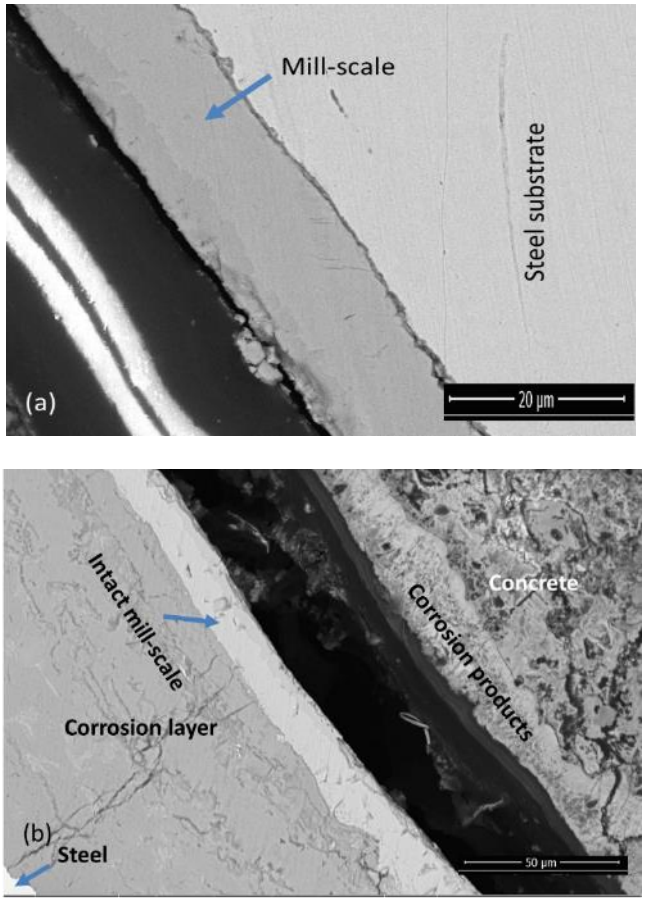

Fig. 8. Mill-scale of corroded steel reinforcement after applying impressed current method-(a) intact mill-scale without trace of corrosion and (b) mill-scale sandwiched between corrosion layer and corrosion products.

On side (1), where the corrosion was visibly less severe, the mill-scale is either randomly observed as prior applying the impressed current (whether intact or fractured) or sandwiched between the corrosion layer and corrosion products, as indicated in Fig. 8(a) and Fig. 8(b), respectively. Note that the corrosion layer is the layer formed by the corrosion of steel beneath the mill-scale and still located at the original location, as described in Fig. 8(b), while the corrosion products assigned for the products formed from the oxidization and then dissolution of steel and then accumulated into a dense layer in concrete adjacent the steel-concrete interfacial region. The corrosion layer can be identified easily based on its brightness. Compared to mill-scale layer and steel substrate, the brightness of corrosion layer under SEM is obviously lower. The thickness of corrosion layer formed beneath the mill-scale was estimated by the perpendicular distance from the mill-scale remnant to the steel substrate. Obviously, the thickness of corrosion layer was inconsistent, as expressed in Figs. 9 to 11. It can vary from few to hundreds µm. EDS analyses indicated that the Fe/O ratios of the corrosion layer was highly consistent, approximately 0.665±0.025. Notably, chloride ions were hardly detected in this corrosion layer. It was in contrast to previous study where the chloride ions were detected in corrosion layer after the corrosion acceleration was conducted by using artificial climate environment [13]. In addition, corrosion products in the concrete region adjacent to the steel-concrete interfacial region probably formed due to the penetration of them from corroded regions and then accumulated at the concrete adjacent. The concrete area contaminated with corrosion products contained higher content of Fe in its chemical composition than bulk concrete, where there was without contamination of corrosion products. Therefore, the area where corrosion product penetrated into can be identified easily based on its brightnes under SEM. EDS analyses expressed that the corrosion products here possessed about 0.2-0.5% wt chloride.

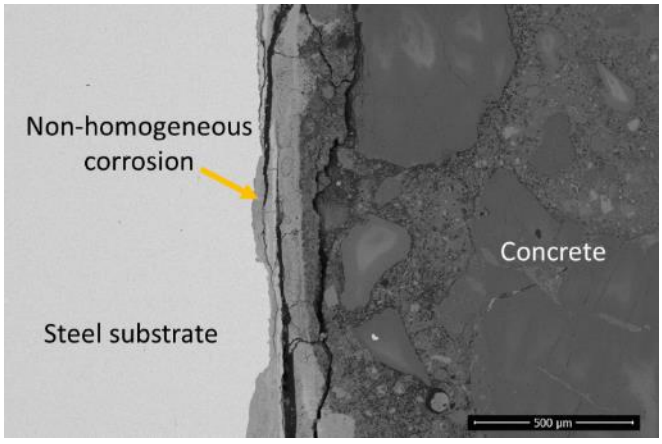

Fig. 9. Non-homogeneous corrosion induced by impressed current.

On side (2), which faced the cathode and NaCl solution directly during the application of impressed current, it is interesting that the corrosion appears to be non-homogeneous, as indicated in Fig. 9. The general corrosion and localized corrosion are coexistent, as presented in Fig. 10 and Fig. 11. The localized corrosion happens to be analogue to the pitting corrosion of steel reinforcement in the reinforced concrete structures exposing chloride environment, as presented in Fig. 10. The Fe/O ratios of this corrosion products varied extensively depending upon the detecting location. At the region adjacent the pit of localized areas in Fig. 10(a) (the end of red arrow), the Fe/O ratio changed widely, from 0.52 to 10, but mostly in the range of 0.74-0.92. That was the intermixing of various phases of iron with different oxidization state (corroded and non-corroded). And the oxidization state of +2 was deemed to be dominant. The remains of steel in the interaction volume between electron beam and the material of EDS analysis [11] is probably one of the causes for that wide range of Fe/O ratio. In contrast, there are regions where localized corrosion was more severely corroded, as presented in Fig. 10(b). The Fe/O ratio of corrosion layer adjacent the pit of these localized corrosion regions was meaningfully consistent, approximately 0.5-0.8. These regions were apparently oxidized to a higher state compared to the localized corrosion region showed in

Fig. 10(a). Chloride ions were detected in this layer with the content of 1.2-2% wt. The corrosion layer in the area where general corrosion happened, as presented in Fig. 11, appears with marble structure and the thickness varies widely, from hundreds μm to 1.0 mm. The marble structure of corrosion layer includes patterns with different levels of brightness where the bright regions owned the Fe/O ratio of approximately 0.65-0.82 and the dark regions possessed the Fe/O ratio of 0.5 to 0.72. This observation is in line with Chitty et al. [34] where the corrosion products appeared with similar marble structure. The existence of Fe/O ratio of 0.5 suggests that the corrosion products in this layer probably containing iron oxy-hydroxide FeOOH. Chloride ions were detected with content of 3-8% wt, meaningfully higher compared to those at the localized corrosion. Interestingly, the severe corrosion of steel reinforcement resulting in the volume expansion is able to fracture and crack the mill-scale at different level, as expressed in Fig. 10 and Fig. 11. However, based on the EDS results taken on mill-scale after applying impressed current, the electric current is unable to change the mill-scale's composition. Furthermore, the thickness of mill-scale after corrosion is approximately 15-20 μm, as presented in Fig. 8(b), Fig. 10(b) and Fig. 11. This thickness seems unchanged compared to the non-corroded steel reinforcement. Probably, the mill-scale was non-expansive due to the corrosion induced by impressed current method. Considering the corrosion products accumulated at the concrete adjacent steel-concrete interfacial region, in contrast to the variable Fe/O ratio of corrosion layer, the corrosion products appeared with a greatly consistent Fe/O ratio of about 0.5 with the high contamination of chloride, approximately 3.5-8% wt.

Likely to natural corrosion, goethite (α-FeOOH) and lepidocrocite (γ-FeOOH) [35-38] were easily observed at the corrosion layer as well as corrosion products, as presented in Figs. 12(a) and 12(b). Furthermore, akaganeite (β-FeOOH) which considered as typical corrosion product appeared on the structure exposing chloride environment, was also spotted beside magnetite (Fe_3O_4), as shown in Fig. 12(c) [9, 39]. The existence of these phases is a positive sign supporting the application of impressed current method for corrosion acceleration.

Nossoni et al. [21] suggested that unlike the natural corrosion process, where anodic reaction was always the oxidization of iron, when the impressed current was applied, the anodic reactions occurred on the steel reinforcement greatly depended upon the ratio of Cl^-/OH^- of the electrolyte, the pore solution in concrete. Since the concentration of chloride ions in pore solution was minor and insignificant compared to concentration of hydroxide ions, the oxidation the steel rebar seemed to be unable to occur. Instead, hydroxide ions which were abundant in the pore solution oxidized on the mill-scale, as presented in Eq. (2), in order to maintain the electric current. Nevertheless, since the chloride concentration increased, the steel reinforcement began to oxidize, as shown in Eq. (3). The electric current was then maintained by both oxidation of hydroxide ions and iron until the Cl^-/OH^- ratio reached the critical value, which was assumed to be approximately 0.5-0.6, the oxidation of iron is the main anodic reaction.

$$2OH^- \rightarrow (1/2)O_2 + H_2O + 2e \quad (2)$$

$$Fe \rightarrow Fe^{2+} + 2e \quad (3)$$

The formation of non-uniformed and non-homogeneous corrosion layers induced by the impressed current in this research seems in well agreement with those suggestions. On the region where chloride was not detected, hydroxide ions in pore solution of concrete probably oxidized instead of the steel, leading to the preservation of mill-scale without trace of corrosion layer, as shown in Fig. 8(a). Oxygen generating from OH^- oxidation, as shown in Eq. (2), happened to be a severe risk. It can penetrate in the fractured mill-scale, triggering the corrosion of steel and reasonably forming the corrosion layer with immeasurable trace of chloride. In contrast, the corrosion of steel, as presented in Eq. (3) was probably the main oxidization reaction at the region the steel exposed chloride ions, leading to the localized corrosion which is analogous to pitting corrosion, and then forming a corrosion layer contained high chloride content. Conclusively, the impressed current method was able to induce nonhomogeneous corrosion of steel in reinforced concrete. However, unlike the corrosion process which usually happens with the deficiency of oxygen, the oxidation of hydroxide ions at non-chloride region was able to generate oxygen, forming an abundant oxygen environment for the further corrosion of steel. The abundant oxygen and the high electric voltage of impressed current are able to oxidize iron to the higher state than natural corrosion.

Figure 13 presents the backscatter electron image and mapping analysis images of iron, calcium, silicon and aluminum at the concrete adjacent to steel-concrete interface. The concrete region which intruded by corrosion products is clearly brighter than the concrete region far away in backscatter electron images. Obviously, it is due to the higher mean atomic number. Figures 11 and 13 show that the corrosion products can penetrate far into concrete with non-uniform extent and able to reach about 1 mm. The extent of penetration probably depends on the concrete properties at steel-concrete interfacial region such as the porosity and size of aggregates. The existence of aggregates at this concrete region seems able to enhance the penetration of corrosion products. Iron ions can intrude far into concrete through the transition zone between paste and aggregate. It is confirmed by EDX in Fe mapping image in Fig. 13. The huge extent of the corrosion product penetration into concrete is in contrast with the previous studies where the experiments were conducted on natural corrosion or using the artificial climate environment to accelerate the corrosion. In these previous studies, the extent of iron ions penetrated into concrete appeared relatively unchanged with the increase of corrosion level,

being approximately 200 μm [10, 40]. The greatly higher of the extent of corrosion product penetration is probably due to the difference of penetration mechanism. While the penetration of iron ions into concrete caused by natural corrosion or artificial climate acceleration is mainly due to the diffusion of the green complexes containing Cl^-, Fe^{2+} and Fe^{3+} [10], it is the migration of the iron ions under the impact of electric field, which is generated by the electric current when the impressed current method is used to induce the corrosion. This electric field can push iron ions away the anode, and then enhancing the penetration of iron ions into the bulk concrete region. The reduction of calcium and silicon in cement paste at corrosion-product intruded concrete region compared to the concrete region far away is also observed, as shown in the Ca mapping and Si mapping (Fig. 13). While the decalcification of cement paste at the corrosion-product intruded region is alleged to the cause of the calcium reduction at the corrosion-product intruded region, which is in line with the previous studies [10, 41, 42], the cause of the silicon reduction is still unclear.

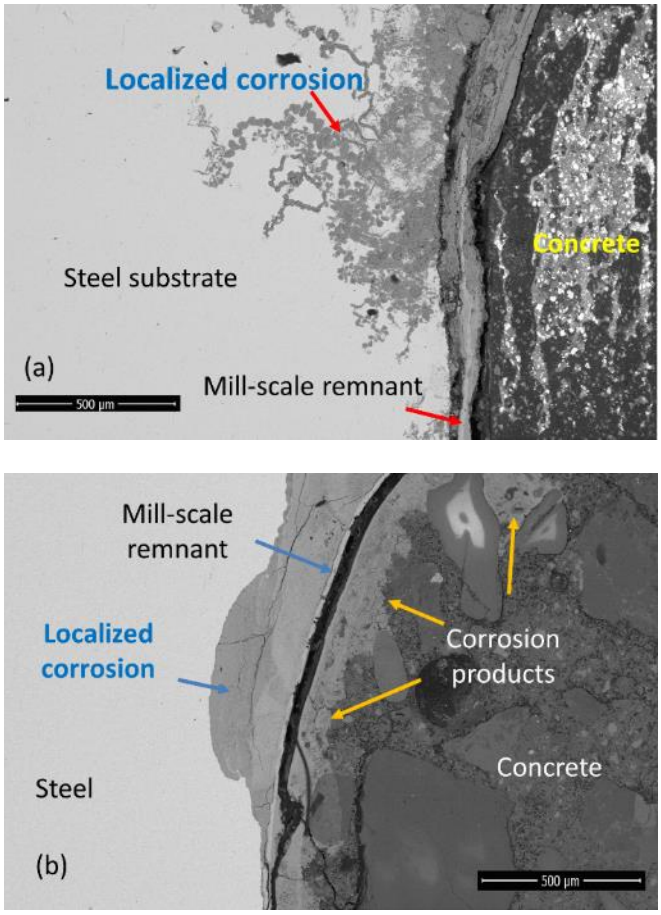

Fig. 10. Localized corrosion in steel reinforcement generated by impressed current at (a) low oxidization state and (b) high oxidization state.

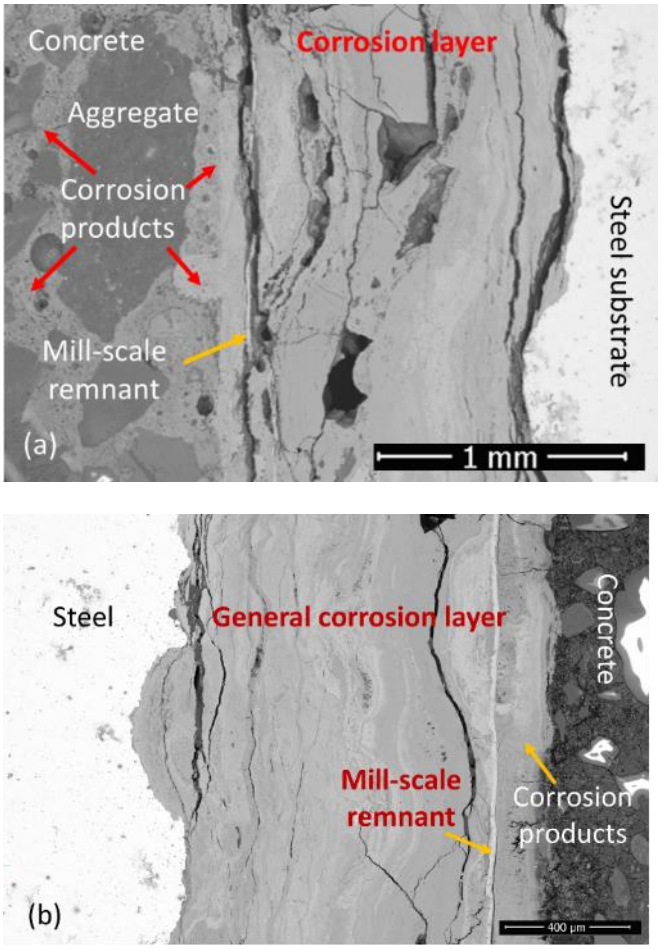

Fig. 11. General corrosion caused by the impressed current with various thickness of corrosion layer (a) ~ 1 mm (b) ~ 400 μm.

It is worth emphasizing that when the steel corroded due to natural cause or accelerated cause by using artificial climate environment, the transition zone at steel-concrete interface was fully infilled by the corrosion products [10, 25, 43] before causing cracks in concrete. Furthermore, the corrosion products penetrated into concrete with a relatively unchanged extent, being approximately 200 μm [10, 25, 43]. However, when the corrosion was induced by the impressed current method, the gap between steel and concrete is still observed and the extent of penetration is much higher than natural corrosion, approximately 500 μm or more, as presented in Fig. 10 and Fig. 13. This steel-concrete transition gap seems only infilled at the location the corrosion layer reaches to the size of 1 mm, supposed to be severely corroded, as indicated in Fig. 11. These meaningful contrasts are obviously caused by the difference in corrosion-induced mechanisms. The use of impressed current can help to push iron ions away the anode and enhance the penetration of iron ions into concrete. Furthermore, the oxidization of hydroxide OH^- ions at the anode, as presented in Eq. (2) can reduce the hydroxide concentration in the electrolyte at the gap space (transition zone) between the steel and concrete, neutralizing/acidizing the electrolyte there and then,

inhibiting the precipitation of corrosion products at that gap. Consequently, it can slow down the formation of cracks in concrete and therefore, lead to the overestimation of load capacity of corroded structure. Notably, the use of electric current can deteriorate C-S-H in cement paste [18], which seems to be the cause for the reduction silicon in corrosion-product intruded region.

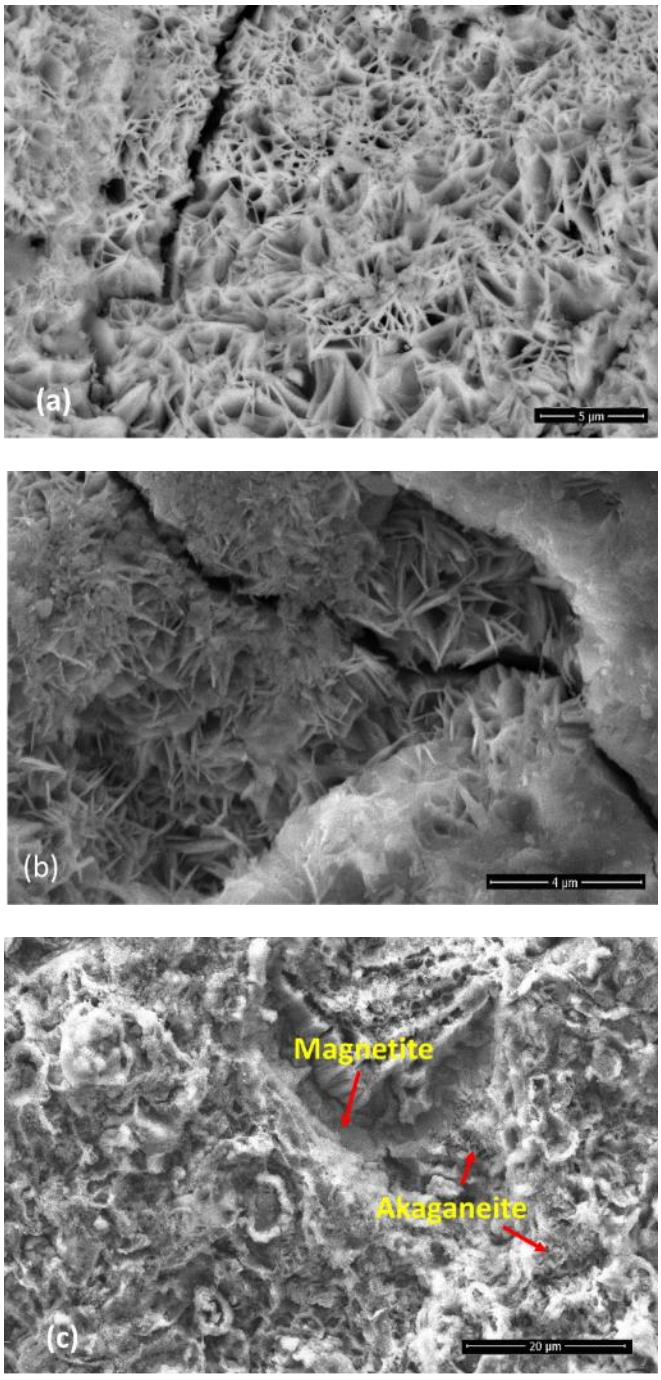

Fig. 12. Corrosion products observed at steel surface (a) Goethite (α-FeOOH) (b) Lepidocrocite (γ-FeOOH) and (c) Akaganeite (β-FeOOH) and magnetite .

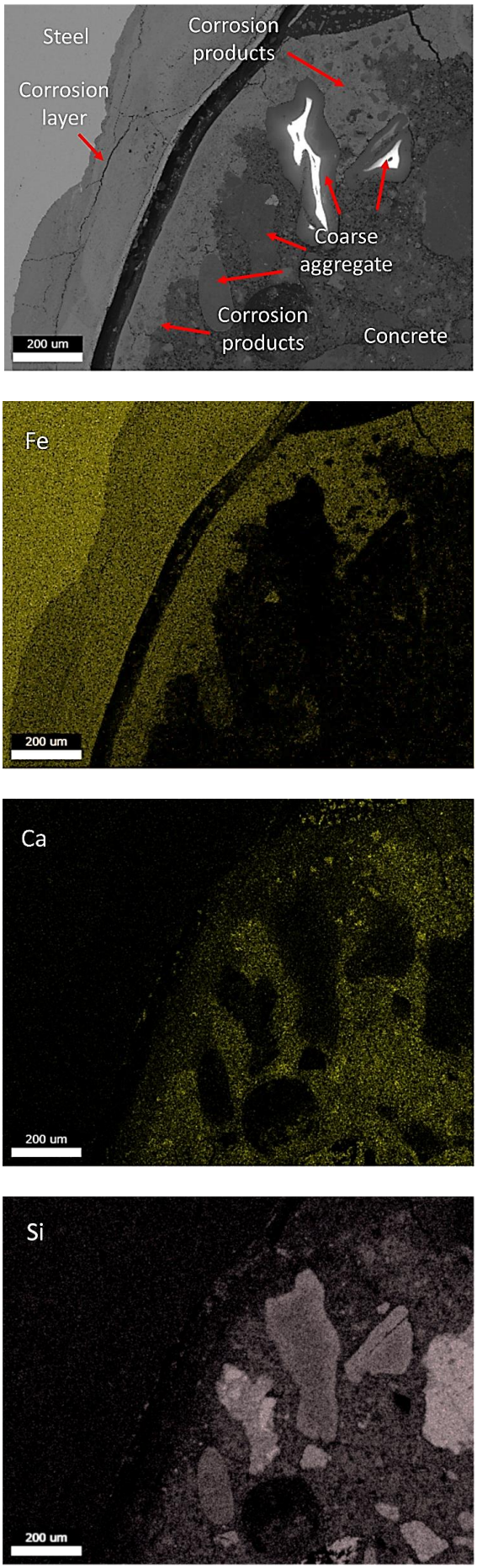

Fig. 13. Penetration of corrosion products into concrete and EDX-mapping of main elements in concrete at steel-concrete interfacial region

4. Conclusions

The characterization of steel mill-scale and the behavior of steel-concrete interfacial region in the reinforced concrete corroded by employing impressed current method were investigated to validate the reliability of this method in terms of simulating the natural corrosion. Based on the results observed, the following conclusions can be drawn:

- Mill-scale on the surface of non-corroded steel was not fully intact but appeared randomly fractured. These fractured defects are more likely to be an initially imperfect characteristic of mill-scale of steel reinforcement. After applying impressed current method, the chemical composition and the thickness of mill-scale were deemed to be unchanged.
- The non-uniform and localized corrosion on the steel reinforcement can be induced by applying the impressed current method.
- Goethite and Lepidocrocite were easily observed on corroded steel. Akaganeite, which is the typical corrosion product formed at corroded steel of reinforced concrete structure exposed chloride environment was also detected.
- The precipitation of corrosion products at steel-concrete transition zone was inhabited. It can slow down the formation of cracks in concrete and then overestimate the load capacity of corroded reinforced concrete structure.

Based on these points, it is reasonable to state that impressed current method seems inappropriate to be used as a reliable method to simulate the natural corrosion on reinforced concrete structure exposed to chloride environment. Particularly, the impressed current method may not be recommended for the studies aiming to characterize the interaction between corrosion products and cement paste, the accumulation of corrosion products at steel-concrete transition region as well as the formation of cracks in concrete.

Acknowledgement

The research described in this paper was financially supported by Industrial University of Ho Chi Minh City with Grant No. 20/1.2XD01.

References

[1] A. Poursaee, "Corrosion of steel in reinforced concrete structures," in *Woodhead Publishing Series in Civil and Structural Engineering*, 1st Edition, 2016.

[2] P. V. Bahekar and S. S. Gadvea, "Corrosion of rebar in carbon fiber reinforced polymer bonded reinforced concrete," *Advances in Concrete Construction*, vol. 8, no. 4, pp. 247-255, 2019. [Online]. Available: https://doi.org/10.12989/acc.2019.8.4.247

[3] P.G. Malerba, L. Sgambi, D. Ielmini, and G. Gotti, "Influence of corrosive phenomena on bearing capacity of RC and PC beams," *Advances in Concrete Construction*, vol. 5, no. 2, pp. 117-143, 2017. [Online]. Available: https://doi.org/10.12989/acc.2017.5.2.117

[4] U. Angst, "Chloride induced reinforcement corrosion in concrete: Concept of critical chloride content - methods and mechanisms," Thesis for the degree of Philosophiae Doctor, Norwegian University of Science and Technology, 2011.

[5] L. Djeddi and A. Amirat, "Corrosion initiation time models in RC coastal structures based on reliability approach," *Advances in Concrete Construction*, vol. 9, no. 2, pp 149-159, 2020. [Online]. Available: https://doi.org/10.12989/acc.2020.9.2.149

[6] T. Luping, "Chloride ingress in concrete exposed to marine environment - Field data up to 10 years' exposure," SP Swedish National Testing and Research Institute, 2003.

[7] C. M. Hansson, A. Poursaee, and S. J. Jaffer, "Corrosion of reinforcing bars in concrete," Portland Cement Association (PCA), PCA R&D Serial No. 3013, 2007.

[8] A. K. Azad, S. Ahmad, and S. A. Azher, "Residual strength of corrosion-damaged reinforced concrete members," *ACI Materials Journal*, vol. 104, pp. 303-310, 2007.

[9] D. A. Koleva, J. Hu, A. L. A. Fraaij, P. Stroeven, N. Boshkov, and J. H. W. De Wit, "Quantitative characterisation of steel/cement paste interface microstructure and corrosion phenomena in mortars suffering from chloride attack," *Corrosion Science*, vol. 48, pp. 4001-4019, 2006.

[10] H. Wong, Y. Zhao, R. Karimia, N. Buenfelda, and W. Jinb, "On the penetration of corrosion products from reinforcing steel into concrete due to chloride-induced corrosion," *Corrosion Science*, vol. 52, pp. 2469-2480, 2010.

[11] T. H. Y. Nguyen, K. Tsuchiya, D. Atarashi, "Microstructure and composition of fly ash and ground granulated blast furnace slag cement pastes in 42-month cured samples," *Construction and Building Materials*, vol. 191, pp. 114-124, 2018. [Online]. Available: https://doi.org/10.1016/j.conbuildmat.2018.09.206

[12] T. H. Y. Nguyen, K. Tsuchiya, D. Atarashi, and H. Yokota, "Electrokinetic properties and mechanism of chloride binding in 42-month cured cement pastes with fly ash and ground granulated blast furnace slag exposed to seawater," *Construction and Building Materials*, vol. 240, p. 117944, 2020. [Online]. Available: https://doi.org/10.1016/j.conbuildmat.2019.117944

[13] E. Rossi, R. Polder, O. Copuroglu, T. Nijland, and B. Šavija, "The influence of defects at the steel/concrete interface for chloride-induced pitting corrosion of naturally-deteriorated 20-years-old specimens studied through X-ray Computed Tomography," *Construction and Building Materials*, vol. 235, p. 117474, 2020.

[14] A. Scott and M. G. Alexander, "Effect of supplementary cementitious materials (binder type) on the pore solution chemistry and the corrosion of steel in alkaline environments," *Cement and Concrete Research*, vol. 89, pp. 45-55, 2016.

[15] Y. Wang, F. Gong, D. Zhang, and T. Ueda, "Estimation of ice content in mortar based on electrical measurements under freeze-thaw cycle," *Journal of Advanced Concrete Technology*, vol. 14, pp. 35-46, 2016.

[16] V. H. L. Bui, S. Boonchai, and T. Ueda, "Ductility of concrete beams reinforced with both FRP and steel tension bars," *Journal of Advanced Concrete Technology*, vol. 16, pp. 531-548, 2018.

[17] T. H. Y Nguyen, W. Pansuk, and P. Sancharoen, "The effects of electro-chemical chloride extraction on the migration of ions and the corrosion state of embedded steel in reinforced concrete," *KSCE Journal of Civil Engineering*, vol. 22, pp. 2942-2950, 2018. [Online]. Available: https://doi.org/10.1007/s12205-017-2022-7

[18] T. H. Y. Nguyen, H. Yokota, and K. Hashimoto, "Effects of electrochemical chloride extraction on hydrated products of various cement paste systems," *Journal of Advanced Concrete Technology*, vol. 13, pp. 564-582, 2015. [Online]. Available: https://doi.org/10.3151/jact.13.564

[19] S. Care and A. Raharinaivo, "Influence of impressed current on the initiation of damage in reinforced mortar due to corrosion of embedded steel," *Cement and Concrete Research*, vol. 37, pp. 1598-1612, 2007.

[20] S. Care, Q. T. Nguyen, V. L'Hostic, and V. Berhaud, "Mechanical properties of the rust layer induced by impressed current method in reinforced mortar," *Cement and Concrete Research*, vol. 38, pp. 1079-1091, 2008.

[21] G. Nossoni and R. Harichandran, "Current efficiency in accelerated corrosion testing of concrete," *Corrosion*, vol. 68, pp. 801-809, 2012.

[22] T. Maaddawy and K. Soudki, "Effectiveness of impressed current technique to simulate corrosion of steel reinforcement in concrete," *Journal of Materials in Civil Engineering*, vol. 15, pp. 41-47, 2003.

[23] C. V. Nguyen and P. Lambert, "Effect of current density on accelerated corrosion of reinforcing steel bars in concrete," *Structure and Infrastructure Engineering*, vol. 14, pp. 1535-1546, 2018.

[24] D. Qiao, H. Nakamura, Y. Yamamoto, and T. Miura, "Crack patterns of concrete with a single rebar subjected to non-uniform and localized corrosion," *Construction and Building Materials*, vol. 116, pp. 366-377, 2016.

[25] Y. Zhao, Y. Wu, and W. Jin, "Distribution of millscale on corroded steel bars and penetration of steel corrosion products in concrete," *Corrosion Science*, vol. 66, pp. 160-168, 2013.

[26] W. Zhang, J. Chen, X. Luo, "Effects of impressed current density on corrosion induced cracking of concrete cover," *Construction and Building Materials*, vol. 204, pp. 213-223, 2019.

[27] H. Ye, C. Fu, N. Jin, and X. Jin, "Performance of reinforced concrete beams corroded under sustained service loads: A comparative study of two accelerated corrosion Techniques," *Construction and Building Materials*, vol. 162, pp. 286-297, 2018.

[28] C. Andrade, C. Alonso, and F. J. Molina, "Cover cracking as a function of bar corrosion: Part 1 – Experimental test," *Materials and Struc*ture, vol. 26, pp. 453-464, 1993.

[29] S. A. Austin, R. Lyons, and M. J. Ing, "Electrochemical behavior of steel-reinforced concrete during accelerated corrosion testing," *Corrosion*, vol. 60, no. 2, pp. 203-212, 2004.

[30] G. Malumbela, M. Alexander, and P. Moyo, "Interaction between corrosion crack width and steel loss in RC beams corroded under load," *Cement and Concrete Research*, vol. 40, pp. 1419-1428, 2010.

[31] J. Bilcik and I. Holly, "Effect of reinforcement corrosion on bond behaviour," *Procedia Engineering*, vol. 65, pp. 248-253, 2013.

[32] W. Melfo and R. J. Dippenaar, "In situ observations of early oxide formation in steel under hot-rolling conditions," *Journal of Microscopy*, vol. 225, pp. 147-155, 2007.

[33] P. Lazor, O. Shebanova, and H. Annersten, "High-pressure study of stability of magnetite by thermodynamic analysis and synchrotron X-ray," *Journal of Geophysical Research*, vol. 109, p. B05201, 2004.

[34] W. Chitty, P. Dillmann, V. L'Hostis, and C. Lombard, "Long-term corrosion resistance of metallic reinforcements in concrete-a study of corrosion mechanisms based on archaeological artefacts," *Corrosion Science*, vol. 47, pp. 1555-1581, 2005.

[35] A. Raman, S. Nasrazadani, and L. Sharma, "Morphology of rust phases formed on weathering steels in various laboratory corrosion tests," *Metallography*, vol. 22, pp. 79-96, 1989.

[36] M. Morcillo, B. Chico, J. Alcantara, I. Diaz, R. Wolthuis, and D. Fuentea, "SEM/micro-raman characterization of the morphologies of marine atmospheric corrosion products formed on mild steel," *Journal of the Electrochemical Society*, vol. 163, no. 8, pp. C426-C439, 2006.

[37] R. Antunes, R., Ichikawa, L. Martinez, and I. Costa, "Characterization of corrosion products on carbon steel exposed to natural weathering and to accelerated corrosion tests," *International Journal of Corrosion*, 2014, Article ID 419570.

[38] J. Alcantara, B. Chico, I. Diaz, D. Fuente, and M. Morcillo, "Airborne chloride deposit and its effect on marine atmospheric corrosion of mild steel," *Corrosion Science*, vol. 97, pp. 74-88, 2015.

[39] D. Fuente, I. Diaz, J. Alcantara, B. Chico, J. Simancas, I. Llorente, A. Garcia-Delgado, J.

Jimenez, P. Adeva, and M. Morcillo, "Corrosion mechanisms of mild steel in chloride-rich atmospheres," *Materials and Corrosion*, vol. 67, pp. 227-238, 2016.
[40] B. Browne, "Mechanism of corrosion of steel in concrete in relation to design, inspection, and repair of offshore and coastal structures," *ACI*, vol. SP-65, pp. 169-204, 1980.
[41] G. Glass, B. Reddy, and N.R. Buenfeld, "Corrosion inhibition in concrete arising from its acid neutralisation capacity," *Corrosion Science*, vol. 42, pp. 1587-1598, 2000.
[42] A. Delagrave, M. Pigeon, J. Marchand, and E. Revertegat, "Influence of chloride ions and pH level on the durability of high performance cement pastes (part II)," *Cement and Concrete Research*, vol. 26, pp. 749-760, 1996.
[43] Y. Zhao, J. Yu, B. Hu, and W. Jin, "Crack shape and rust distribution in corrosion-induced cracking concrete," *Corrosion Science*, vol. 55, pp. 385-393, 2012.

Thi Hai Yen Nguyen, photograph and biography not available at the time of publication.

Van Hong Linh Bui, photograph and biography not available at the time of publication.

Van Mien Tran, photograph and biography not available at the time of publication.

Nguyen Thi Cao, photograph and biography not available at the time of publication.

Withit Pansuk, photograph and biography not available at the time of publication**.**

Pitcha Jongvivatsakul, photograph and biography not available at the time of publication.